Chapter 4

On discretisation schemes for a boundary integral model of stochastic ray propagation

Janis Bajars and David J. Chappell

School of Science & Technology,
Nottingham Trent University
Nottingham
UK

Abstract. *A boundary integral operator method for stochastic ray tracing in billiards was recently proposed in [1]. In particular, a phase-space boundary integral model for propagating uncertain ray or particle flows was described and shown to interpolate between deterministic and random models of the flow propagation. In this work we describe discretisation schemes for this class of boundary integral operators using piecewise constant collocation in the spatial variable and either the Nyström method or the collocation method in the momentum variable. The simplicity of the spatial basis means that the corresponding spatial integration can be performed analytically. Convergence properties of the discretisation schemes and strategies for numerical implementation are presented and discussed.*

4.1 Introduction

Boundary integral formulations for propagating particle or ray densities along ray trajectories in computer graphics applications are often termed the rendering equation [2]. This equation therefore lies at the heart of a wide variety of algorithms, both for applications in computer graphics [2] and beyond [3, 4, 5]. The point of departure for this study stems from the observation that the rendering equation may be formulated using deterministic transfer operators of Frobenius-Perron (FP) type [5, 6]. Replacing the deterministic transfer operator with a stochastic one results in a boundary integral formulation for stochastic propagation of ray densities. The simplest implementation of a stochastic treatment is to assume that rays propagate uniformly with equal probability of all admissible propagated ray vectors. This formulation is known as the radiosity method (with Lambertian reflection) in the room acoustics community [3, 4]. A more widely applicable implementation arises if one assumes that the mapped ray vector is normally distributed, with mean given by the associated deterministic dynamics. The resulting stochastic evolution operator will be of Fokker-Planck type as discussed in [7, 8]. The choice of variance in this approach allows the model to be tuned to the level of uncertainty prescribed by

the application. Example applications arise in fluid dynamics [9], weather forecasting [10], linear wave dynamics or in general in describing the evolution of phase-space densities of a dynamical system.

In this work, we discuss two possible discretisation schemes for a family of boundary integral operators for stochastic ray propagation. Our discretisation strategy is based on a piecewise constant collocation method in the spatial variable, together with an exact integration procedure for the corresponding spatial integral. For the momentum variable we apply the Nyström method, which takes care of the integral over the momentum variable within the discretisation approach, or the collocation method, which separates dependence of the integral over the momentum variable from the discretisation approach. We then discuss the implementation strategies and convergence properties of the discretisation schemes.

4.2 Boundary integral operator model for the stochastic propagation of phase-space densities

Consider phase-space in two-dimensions with position vector $\mathbf{r} \in \mathbb{R}^2$ and momentum (or slowness) vector $\mathbf{p} \in \mathbb{R}^2$. Let Ω denote a finite two-dimensional domain with an associated speed of propagation c. The Hamiltonian $\hat{H} = c|\mathbf{p}| = 1$ describes the ray trajectories within Ω between reflections at the boundary $\Gamma = \partial\Omega$. We write the phase-space coordinates on the boundary of Ω as $X = (s, p)$, where s is an arc-length parametrisation of Γ and $p = c^{-1}\sin(\theta)$ is the tangential component of the momentum vector $\mathbf{p}$ at the point s, where $\theta \in (-\pi/2, \pi/2)$ is the angle between the trajectory leaving the boundary at s and the normal vector to Γ (also at s).

The stochastic propagation of a density ρ through phase-space is described by an operator of the form [1]

$$\mathcal{L}_{\boldsymbol{\sigma}}\rho(X) = \int_Q f_{\boldsymbol{\sigma}}(X - \varphi(X'))\rho(X')\,\mathrm{d}X'. \tag{4.1}$$

Here $Q = \Gamma \times (-c^{-1}, c^{-1})$ denotes the phase-space on the boundary and $\varphi : Q \to Q$ defines the boundary flow map, which maps a vector in Q to another vector in a subset of Q, leading to a deterministic evolution of the form $\varphi(X') = X$, where $X' = (s',\, p')$ and $X = (s, p)$. Geometrically, φ corresponds to the composition of a translation (from s' to s) and a rotation to the direction corresponding to a specular reflection. The kernel of the boundary integral operator (4.1) is given by a probability density function (PDF) $f_{\boldsymbol{\sigma}}$ such that

$$\int_Q f_{\boldsymbol{\sigma}}(X)\,\mathrm{d}X = 1, \tag{4.2}$$

and $\boldsymbol{\sigma}$ is a parameter set controlling its shape.

With reference to applications in vibro-acoustics, this probabilistic behaviour could be attributed to, for example, uncertain fluctuations in the wave speed c, roughness of the reflecting surface or uncertainties in the boundary conditions/source terms. In all cases we assume that the total energy $\hat{H} = c|\mathbf{p}| = 1$ remains fixed and that the total probability is conserved, that is, condition (4.2) holds throughout. Note that in contrast to the models considered in [7, 8], the range of integration in the domains considered here is in general bounded, which has implications for the choice of suitable PDFs $f_{\boldsymbol{\sigma}}$. The simplest case is to take $f_{\boldsymbol{\sigma}} = const$, upon which one arrives at a model describing propagation to all admissible positions and directions with equal probability. The system is thus by definition ergodic and independent of the underlying classical dynamics. In general, we would like to arrive at a stochastic operator which includes both deterministic propagation and the random propagation model described above as limiting cases [1]. In addition, the PDF $f_{\boldsymbol{\sigma}}$ needs to obey conditions on the sampling ranges due to the

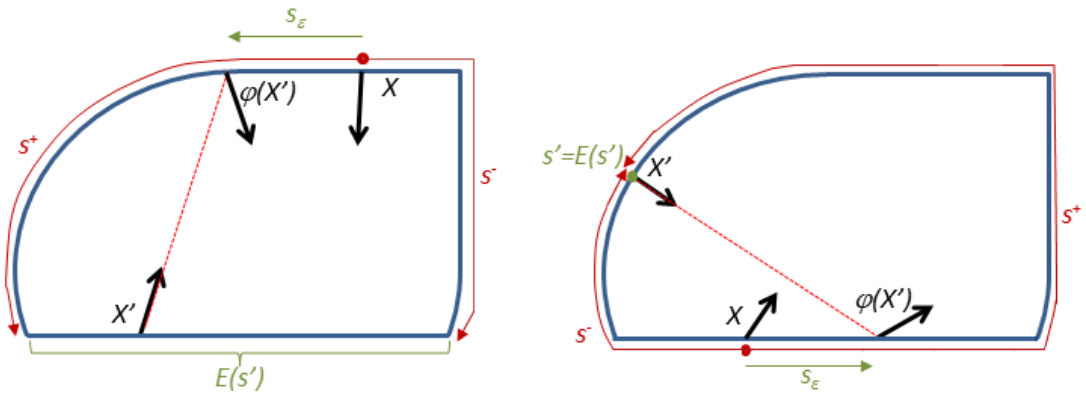

Figure 4.1: Source: Ref. [1]. Tracking ray trajectories via a noisy boundary map and truncation limits $s^\pm$ for the random variable s_ε.

limited range of the boundary map φ. For simplicity, we will restrict to convex domains Ω to avoid additional complications due to incorporating visibility functions.

For an initial boundary distribution ρ_0 on Q, the final equilibrium distribution (including contributions from arbitrarily many reflections) may be computed using the following boundary integral equation (see for example [1] and [5]):

$$(I - \mathcal{L}_{\boldsymbol{\sigma}})\rho = \rho_0. \tag{4.3}$$

Note that for the solution ρ to converge, energy losses must be introduced into the system, which could take place at the boundaries themselves, or along the trajectories. In general, a weight factor w will be added inside the integral in the definition of $\mathcal{L}_{\boldsymbol{\sigma}}$ which contains a dissipative term, and for the extension to multiple domains connected at interfaces w will also contain reflection/transmission probabilities at these interfaces.

We may interpret the evolution given by the operator in Eq. (4.1) as originating from a stochastic boundary map $\varphi_{\boldsymbol{\sigma}}$ with added noise, that is,

$$\begin{aligned} \varphi_{\boldsymbol{\sigma}}(X') &= X \\ &= \varphi(X') + X_\varepsilon, \end{aligned} \tag{4.4}$$

where $X_\varepsilon = (s_\varepsilon, p_\varepsilon)$ are random variables drawn from the PDF $f_{\boldsymbol{\sigma}}$. Note that s_ε is understood as a shift in (anti-clockwise) direction. For $X \in Q$ given, we have to ensure that $\varphi(X') = X - X_\varepsilon$ is in the range of the deterministic map φ; this yields restrictions on the possible values of X_ε and thus on the domain of $f_{\boldsymbol{\sigma}}$.

We express $\varphi = (\varphi_s, \varphi_p)$ in terms of its position and momentum components and again write the initial coordinate as $X' = (s', p')$. The range of admissible values for $\varphi_s(X')$ is $[0, L) \setminus E(s')$, where $E(s')$ is the (closed) set of all points on the same straight edge as s', see Fig. 4.1. Note that for curved edges we set $E(s') = s'$ as shown in the right plot of Fig. 4.1. Furthermore, we have that $\varphi_p(X') \in (-c^{-1}, c^{-1})$. It is therefore necessary to truncate the ranges from which X_ε are sampled to the ranges where for fixed X, $\varphi(X') \in ([0, L) \setminus E(s')) \times (-c^{-1}, c^{-1})$ in Eq. (4.4). Denoting these truncated ranges by (X^-, X^+) where $X^\pm = (s^\pm, p^\pm)$, the PDF $f_{\boldsymbol{\sigma}}$ will have support on $X_\varepsilon \in (X^-, X^+)$ only. A cut-off function $\chi(X_\varepsilon; X^-, X^+)$ for restricting the support of $f_{\boldsymbol{\sigma}}$ to (X^-, X^+) can be defined in the usual way using Heaviside step functions. Having obtained the domain of the PDF, we can now derive a PDF from an uncorrelated bivariate Gaussian distribution with mean $\mathbf{0} = (0, 0)$ and standard deviation $\boldsymbol{\sigma} = (\sigma_1, \sigma_2)$. A scaled PDF

is obtained by setting

$$f_{\boldsymbol{\sigma}}(X_\varepsilon; X^-, X^+) = \frac{\chi(X_\varepsilon; X^-, X^+) \exp\left(-\frac{s_\varepsilon^2}{2\sigma_1^2}\right) \exp\left(-\frac{p_\varepsilon^2}{2\sigma_2^2}\right)}{2\pi\sigma_1\sigma_2\psi_{\sigma_1}(s^-, s^+)\psi_{\sigma_2}(p^-, p^+)}, \tag{4.5}$$

where the scaling defined through ψ_{σ_1} and ψ_{σ_2} is given as

$$\psi_{\sigma_1}(s^-, s^+) = \frac{1}{2}\left(\operatorname{erf}\left(\frac{s^+}{\sqrt{2}\sigma_1}\right) - \operatorname{erf}\left(\frac{s^-}{\sqrt{2}\sigma_1}\right)\right), \tag{4.6}$$

and ψ_{σ_2} is defined analogously. The scaling ensures that the PDF satisfies condition (4.2) for the truncated sampling ranges specified through χ. Note that the mean and variance of $f_{\boldsymbol{\sigma}}$ differs in general from that of the underlying Gaussian distribution, but can be computed from the PDF (4.5) using standard formulae.

Taking the limit of (4.5) as $\boldsymbol{\sigma} \to \mathbf{0}$ then the distribution becomes increasingly sharp and the bivariate Gaussian tends to a two-dimensional delta distribution localised around $X_\varepsilon = X - \varphi(X') = \mathbf{0}$, which leads to a deterministic model. Taking the limit as σ_1, and σ_2 go to ∞ and using the leading order asymptotic expansion of the error function about 0 returns a uniform distribution for $s_\varepsilon \in (s^-, s^+)$ and $p_\varepsilon \in (p^-, p^+)$, leading to the fully stochastic regime described above. See [1] for a more complete discussion of the behaviour of $f_{\boldsymbol{\sigma}}$ in the limit of small and large $\boldsymbol{\sigma}$.

4.3 Discretisation of the boundary integral operator

In this section we detail the approximation of the boundary integral operator (4.1) and the energy density $\rho(X)$, where $X = (s, p)$ as before. We begin our presentation with the discretisation using a piecewise constant collocation method in the spatial variable s and a Nyström method for the momentum variable p. Consider an N-sided closed convex polygon with boundary Γ and a local subdivision of each edge into a number of boundary elements. Then the approximation of the energy density $\rho(X)$ on the boundary Γ may be written

$$\rho(X) = \sum_{j=1}^{n} b_j(s)\rho_j(p), \tag{4.7}$$

where $n \geq N$ is the total number of boundary elements, $\rho_j(p)$ are a set of directionally dependent expansion functions to be determined and $b_j(s)$ are piecewise constant spatial basis functions, i.e. $b_j(s) = 1$ if s lies on the jth element and zero elsewhere.

Substituting (4.7) into (4.1) we obtain

$$\begin{aligned} \mathcal{L}_{\boldsymbol{\sigma}}\rho(X) &= \sum_{j=1}^{n} \int_Q f_{\boldsymbol{\sigma}}(X - \varphi(X'))\rho_j(p')b_j(s')\,\mathrm{d}X' \\ &= \sum_{j=1}^{n} \int_{-c^{-1}}^{c^{-1}} \rho_j(p') \left[\int_{e_j} f_{\boldsymbol{\sigma}}(X - \varphi(X'))\,\mathrm{d}s'\right] \mathrm{d}p', \end{aligned} \tag{4.8}$$

where e_j denotes integration over the jth boundary element. Note that the spatial integral with respect to s' appearing in (4.8) can be solved analytically in terms of the error function erf; this remains tractable if we include an additional damping factor of the form $\exp(-\mu d(s, s'))$, where $\mu \geqslant 0$ is a (viscous) damping parameter and $d(s, s')$ denotes the Euclidean distance between the boundary points s' and s. In what follows, we denote this spatial integral as S_μ, where

$$S_0(s, p') = -\frac{\chi_{s'}}{2\psi_{\sigma_1}} \operatorname{erf}\left(\frac{s - s'}{\sqrt{2}\sigma_1}\right)\Bigg|_{s'=S'_{\min}(p')}^{s'=S'_{max}(p')} \tag{4.9}$$

for the undamped case when $\mu = 0$.

We now change the variable in the momentum integration from $p = c^{-1}\sin(\theta)$ to the direction angle θ and define collocation points s_i, $i = 1, ..., n$, where s_i is chosen as the centroid of the ith boundary element. First, note that the PDF $f_{\boldsymbol{\sigma}}$ defined in Eq. (4.5) can be separated into spatially dependent and directionally dependent components of the form

$$f_{\boldsymbol{\sigma}}(s_\epsilon, p_\epsilon) = \left(\chi_s \frac{\exp\left(-\frac{s_\epsilon^2}{2\sigma_1^2}\right)}{\sqrt{2\pi}\sigma_1\psi_{\sigma_1}}\right)\left(\chi_p \frac{\exp\left(-\frac{p_\epsilon^2}{2\sigma_2^2}\right)}{\sqrt{2\pi}\sigma_2\psi_{\sigma_2}}\right) = f_{\sigma_1}(s_\varepsilon) f_{\sigma_2}(p_\varepsilon).$$

Applying a numerical integration rule such as trapezoidal, Gaussian or Clenshaw-Curtis quadrature with nodes p_k and weights w_k, for $k = 0, ..., K$, then the combined collocation and Nyström method discretisation of equation (4.1) is given by

$$(\mathcal{L}_{\boldsymbol{\sigma}}\rho)(s_i, p_\kappa) = c^{-1} \sum_{j=1, j\neq i}^{n} \sum_{k=0}^{K} w_k \rho_j(\theta_k') f_{\sigma_2}(p_\varepsilon(\theta_k, \theta_k')) S_\mu(s_i, c^{-1}\sin(\theta_k'))\cos(\theta_k'), \tag{4.10}$$

where $i = 1, ..., n$ and $\kappa = 0, ..., K$. The discretisation (4.10) reduces the operator equation (4.3) to a linear system. The solution of this linear system then leads to an approximation for the final equilibrium density distribution ρ given by (4.7), at a set of momenta p_κ, $\kappa = 0, ..., K$.

Notice that the specific set of direction values p_κ in (4.10) are defined by the choice of the numerical quadrature method. In addition, the size of the transfer matrix grows with the number of quadrature nodes. In the small $\boldsymbol{\sigma}$ limit, that is, close to the deterministic dynamics, special numerical quadrature methods could be employed to more efficiently handle the singular perturbation in the PDF as $\sigma_2 \to 0$. In this case, it would be desirable to remove the dependence of the quadrature scheme (for approximating the integral over the momentum variable) from the momentum space discretisation, and hence from the size of the transfer matrix. This is directly achievable by replacing the Nyström method with collocation method in the momentum variable p.

To apply the collocation method in p we consider a finite basis approximation of the directionally dependent functions $\rho_j(p)$ in (4.7)

$$\rho_j(p) = \boldsymbol{\phi}^T(p)\boldsymbol{\rho}_j, \tag{4.11}$$

where $\boldsymbol{\phi}(p) \in \mathbb{R}^{N_p}$ is an N_p dimensional vector of basis functions and $\boldsymbol{\rho}_j \in \mathbb{R}^{N_p}$ are unknown expansion coefficients to be determined for each $j = 1, ..., n$.

Substituting (4.7) together with (4.11) into (4.1) we obtain

$$\mathcal{L}_{\boldsymbol{\sigma}}\rho(X) \;=\; \sum_{j=1}^{n}\left[\int_{-c^{-1}}^{c^{-1}} \boldsymbol{\phi}^T(p') f_{\sigma_2}(p_\varepsilon) S_\mu(s, p')\,\mathrm{d}p'\right]\boldsymbol{\rho}_j.$$

As above we consider spatial collocation points s_i, $i = 1, ..., n$, taken as the centroids of the corresponding boundary elements and introduce directional collocation points p_κ for $\kappa = 1, ..., N_p$. The combined collocation method discretisation of equation (4.1) may therefore be written in the form

$$\begin{aligned}(\mathcal{L}_{\boldsymbol{\sigma}}\rho)(s_i, p_\kappa) &= c^{-1}\sum_{j=1}^{n}\left[\int_{-\pi/2}^{\pi/2} \boldsymbol{\phi}^T(\theta') f_{\sigma_2}(p_\varepsilon(p_\kappa, \theta')) S_\mu(s_i, c^{-1}\sin(\theta'))\cos(\theta')\,d\theta'\right]\boldsymbol{\rho}_j \\ &= \mathbf{v}^T(s_i, p_\kappa)\boldsymbol{\rho}_j \end{aligned} \tag{4.12}$$

with $p_\varepsilon(p_\kappa, \theta') = p_\kappa - c^{-1}\sin(\theta')$ for all $i = 1, ..., n$ and $\kappa = 1, ..., N_p$. In compact matrix notation we may write

$$\Phi\boldsymbol{\rho}_i = V(s_i)\boldsymbol{\rho}_j, \qquad \forall\, i = 1, ..., n,$$

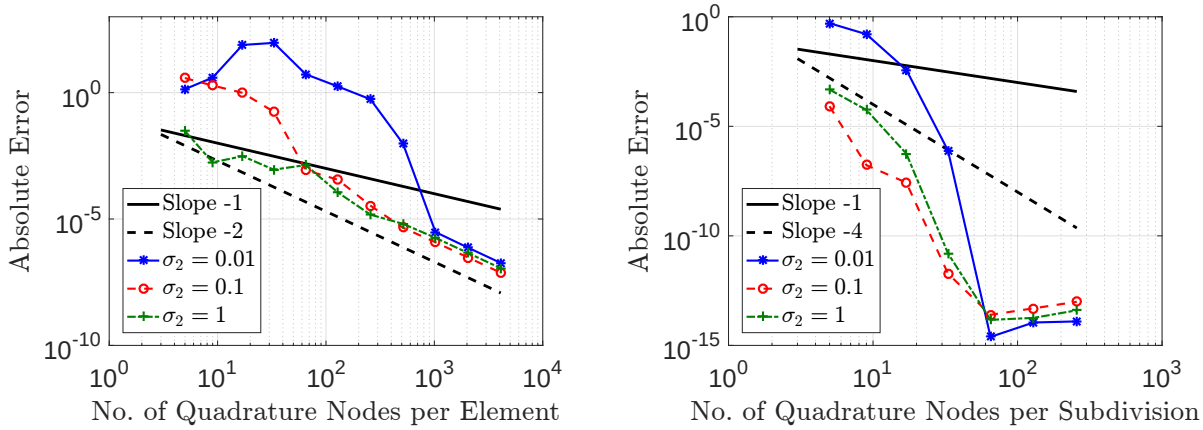

Figure 4.2: Convergence of the integral of the final stationary boundary density along the left hand edge at $x = 0$ for different values of σ_2. Left: using a direct approximation of the integrals over the momentum variable p. Right: using a subdivision strategy for the integral over the momentum variable p. Parameter values: $\sigma_1 = 0$, $c = 1$, $\mu = \pi$ and $n = 8$.

where Φ is a collocation/interpolation matrix with rows $\Phi_\kappa = \boldsymbol{\phi}^T(p_\kappa)$ and $V(s_i)$ is a matrix of integral values with rows given by $V(s_i)_\kappa = \mathbf{v}^T(s_i, p_\kappa)$.

Integrals over the direction angle θ' in (4.12) can be approximated numerically by any desirable quadrature method. Alternatively, special quadrature strategies may be considered for simulations with small σ_2 values due to the singular perturbation as $\sigma_2 \to 0$. In addition, notice that the total size of the transfer matrix compared to the Nyström method above has been changed from $n(K+1) \times n(K+1)$ to $nN_p \times nN_p$. In the next section we discuss and compare different implementation strategies of (4.10) and (4.12) leading to different convergence properties for smooth densities ρ.

4.4 Implementation strategies and convergence properties

In this section, we consider a rectangular domain $(x, y) \in (0, l) \times (0, 0.25)$ where $l = 0.75$, and apply uncertain boundary source term of the form

$$\rho_0(s, p) = \frac{\exp\left(-p^2/(2\sigma_2^2)\right)}{\sqrt{2\pi\sigma_2^2}\,\mathrm{erf}\left(1/(\sqrt{2}\sigma_2 c)\right)} \tag{4.13}$$

along the left hand edge at $x = 0$. A source term (4.13) arising from an uncertain boundary condition was originally proposed in [1]. For small σ_2, this corresponds to a unit boundary density propagating (on average) in the direction $p = 0$, perpendicular to the boundary. For large σ_2 it corresponds to randomly directed propagation from the boundary. Such a condition may be applied for all $s \in \Gamma$, or on a subset of Γ as in [1]. As $\sigma_2 \to 0$, this rectangular domain problem has an analytical ray tracing solution for the stationary interior density $\rho_\Omega(x)$ as detailed in Ref. [11].

In Fig. 4.2 we study the convergence of the integral

$$\mathrm{I} = \int_{-c^{-1}}^{c^{-1}} \rho_j(p)\,\mathrm{d}p = c^{-1}\int_{-\pi/2}^{\pi/2} \rho_j(\theta)\cos(\theta)\,\mathrm{d}\theta = c^{-1}\sum_{k=0}^{K} w_k \rho_j(\theta_k)\cos(\theta_k), \tag{4.14}$$

where $\rho_j(p)$ is the directionally dependent expansion function in (4.7), which we compute along the left hand edge at $x = 0$. The integral is approximated with the same quadrature rule used

in (4.10). We fix the boundary element mesh size taking $n = 8$ elements in total and take parameter values $c = 1$, $\mu = \pi$ and $\sigma_1 = 0$. Note that due to the nature of the exact solution, the spatial dependence of the solution along each edge of the rectangular domain is only slowly varying when σ_1 and σ_2 are relatively small and so a relatively coarse boundary element mesh suffices. The number of quadrature nodes is given by $K_m = 2^m + 1$, where $m = 1, ..., 12$ in the left plot of Fig. 4.2 and $m = 1, ..., 8$ in the right plot of Fig. 4.2. In both plots we plot the absolute error between the integral (4.14) values computed with K_m and K_{m+1} quadrature nodes. The plots show the absolute errors corresponding to the K_{m+1} node number values per element in the left plot and node number values per subdivision in the right plot, respectively.

Note that due to the polygonal nature of the domain and the discontinuous spatial collocation scheme, the direction dependent function S_μ is not continuous over the whole interval, but is at least piecewise smooth. In order to achieve spectral convergence for smooth density solutions in the discretisation schemes presented above, we must subdivide the momentum coordinate integral in (4.8). The left plot of Fig. 4.2 shows the convergence results for different values of σ_2 for a direct approximation of the integral over direction using the Nyström method (4.10) with Gaussian quadrature. This direct approximation of the directional integral leads to the loss of the spectral convergence, and one only obtains second order convergence for a sufficiently large number of quadrature nodes. The right plot shows the convergence results when subdividing the integral over direction and approximating each sub-integral separately via Gaussian quadrature. In this case we do indeed obtain spectral convergence. Equivalent results can also be obtained using the collocation method (4.12).

4.5 Conclusions

We have described a boundary integral model for uncertain high-frequency wave problems and detailed two discretisation schemes for the approximation of the wave energy density. We have discussed implementation strategies to preserve the spectral convergence properties of high order approximation schemes. However, the number of integration subdivisions grows with the number of spatial collocation points and this quadrature data must be saved or constantly recomputed. Furthermore, in the singularly perturbed case $\sigma_2 \to 0$, it would be beneficial to be able to adaptively refine the quadrature to resolve the increasingly sharp peak in the Gaussian PDF. Again, the implementation of such an adaptive scheme in the Nyström method would require a new set of fixed quadrature points for each element. These issues can be directly addressed by instead using a (spectral) collocation method in the momentum variable, which allows for a greater flexibility to tailor the quadrature scheme. Hence, the results presented here serve as motivation to further develop collocation methods for the discretisation in the momentum variable in future.

Acknowledgement

Support from the EPSRC (grant no. EP/M027201/1) and the EU (FP7-PEOPLE-2013-IAPP grant no. 612237 (MHiVec)) is gratefully acknowledged.

References

[1] D. J. Chappell and G. Tanner, *A boundary integral formalism for stochastic ray tracing in billiards*, Chaos, 24(4) (2014), 043147.

[2] J. T. Kayija, The rendering equation. In *Proceedings of SIGGRAPH 1986: 143*, DOI:10.1145/15922.15902.

[3] A. Le Bot, *Energy exchange in uncorrelated ray fields of vibroacoustics*, J. Acoust. Soc. Amer., 120(3) (2006), 1194–1208.

[4] S. Siltanen, T. Lokki, S. Kiminki and L. Savioja, *The room acoustic rendering equation*, J. Acoust. Soc. Amer., 122 (2007), 1624–1635.

[5] G. Tanner, *Dynamical energy analysis - Determining wave energy distributions in vibro-acoustical structures in the high-frequency regime*, J. Sound. Vib., 320 (2009), 1023–1038.

[6] G. Tanner, D. J. Chappell, D. Löchel and N. Søndergaard, *Discrete Flow Mapping: a mesh based simulation tool for mid-to-high frequency vibro-acoustic excitation of complex automotive structures*, SAE Int. J. Passeng. Cars - Mech. Syst., 7(3) (2014), 2014-01-2079.

[7] P. Cvitanović, C. Dettmann, R. Mainieri and G. Vattay, *Trace formulas for stochastic evolution operators: weak noise perturbation theory*, J. Stat. Phys., 93 (1998), 981–999.

[8] D. Lippolis and P. Cvitanović, *How well can one resolve the state space of a chaotic map?*, Phys. Rev. Lett., 104 (2010), 014101.

[9] A. Celani, M. Cencini, A. Mazzino and M. Vergassola, *Active and passive fields face to face*, New Journal of Physics, 6 (2004), 72.

[10] M. Sommer and S. Reich, *Phase-space volume conservation under space and time discretization schemes for the shallow-water equations*, Monthly Weather Review, 138 (2010), 4229–4236.

[11] J. Bajars, D. J. Chappell, N. Søndergaard and G. Tanner, *Transport of phase space densities through tetrahedral meshes using discrete flow mapping*, J. Comp. Phys., 328 (2017), 95–108.

[12] D. J. Chappell and G. Tanner, *Solving the stationary Liouville Equation via a boundary element method*, J. Comp. Phys., 234 (2013), 487–498.